Understanding Mild Acid Pretreatment of Sugarcane Bagasse through Particle Scale Modeling

Running Title:"Microscale Modeling of Bagasse Acid Pretreatment"

Ava A. Greenwood*[1], Troy W. Farrell[1], and Ian M. O'Hara[2]

[1] *Mathematical Sciences, Science and Engineering Faculty, Queensland University of Technology*

[2] *Centre for Tropical Crops and Biocommodities, Queensland University of Technology*

Queensland University of Technology, GPO Box 2432, Brisbane QLD 4001, Australia;
tel: +61 7 3138 2364; fax: +61 7 3138 2310;
e: aa.greenwood@qut.edu.au

*Corresponding author

Abstract

Sugarcane bagasse is an abundant and sustainable resource, generated as a by-product of sugarcane milling. The cellulosic material within bagasse can be broken down into glucose molecules and fermented to produce ethanol, making it a promising feedstock for biofuel production. Mild acid pretreatment hydrolyses the hemicellulosic component of biomass, thus allowing enzymes greater access to the cellulosic substrate during saccharification.

A particle-scale mathematical model describing the mild acid pretreatment of sugarcane bagasse has been developed, using a volume averaged framework. Discrete population-balance equations are used to characterise the polymer degradation kinetics, and diffusive effects account for mass transport within the cell wall of the bagasse. As the fibrous material hydrolyses over time, variations in the porosity of the cell wall and the downstream effects on the reaction kinetics are accounted for using conservation of volume arguments.

Non-dimensionalisation of the model equations reduces the number of parameters in the system to a set of four dimensionless ratios that compare the timescales of different reaction and diffusion events. Theoretical yield curves are compared to macroscopic experimental observations from the literature and inferences are made as to constraints on these 'unknown' parameters. These results enable connections to be made between experimental data and the underlying thermodynamics of acid pretreatment. Consequently, the results suggest that data-fitting techniques used to obtain kinetic parameters should be carefully applied, with prudent consideration given to the chemical and physiological processes being modelled.

Introduction

Sugarcane is a major crop farmed worldwide as a source of sugar (sucrose), which is extracted from the raw sugarcane by a crushing and milling process, followed by various physical and chemical post treatments (Australian Government, 2004).

Bagasse is the fibrous residue of the sugarcane milling process. Current technologies enable cellulosic sugars to be extracted from bagasse, which in turn can be be fermented to produce ethanol suitable for transport fuels. Since bagasse is a low-value by-product of sugarcane milling, it has the advantage of being recognised as a suitable feedstock for 2^{nd} generation biofuels (Nigam and Singh, 2011).

Pretreatment is used in industry to make the cellulose in plant fibres, such as bagasse, more amenable to enzymatic hydrolysis thus improving the yield of fermentable sugars (Olsson et al., 2005; Wyman et al., 2004; Yang and Wyman, 2008b). Hemicelluloses are branched polymers that can be considered to form a monolayer coating around the exterior of cellulose microfibrils (aggregates of linear cellulose chains that are held together by hydrogen bonding), creating a cellulose/xyloglucan network that strengthens the cellulose scaffold (Albersheim et al., 2011; O'Hara et al., 2011; Olsson et al., 2005; Scheller and Ulvskov, 2010).

One pretreatment that is used to remove hemicelluloses from bagasse, is mild acid pretreatment. Under acidic conditions the hemicelluloses are hydrolysed, thus allowing enzymes greater access to the cellulosic substrate during saccharification. The costs associated with pretreatment account for a significant proportion of the projected production costs of bioethanol, and since pretreatment takes place early in the fuel production process, the effectiveness of the pretreatment influences downstream processes and their associated costs. Advances in pretreatment technologies have aided in reducing these production costs in the past (Yang and Wyman, 2008b). Consequently, researching methods to optimise the pretreatment process can help to make the cost of biofuels more commercially viable.

Mathematical modeling can be applied to industrial problems such as biomass pretreatment in order to provide insight into the influence of experimental parameters on process effectiveness and thus help to inform optimal reaction conditions. This is only possible if there is cohesion between the robustness of the model equations and the accuracy of the model parameters.

In the past, variations of the Saemen kinetic model (Saeman, 1945) have commonly been used to describe the hydrolysis of hemicellulose to produce xylose and the subsequent degradation of xylose. Popular variations such as including an oligomer intermediate in the hydrolysis process or splitting the substrate into easy to hydrolyse and hard to hydrolyse classes are discussed in detail by Jacobsen and Wyman (2000). The benefit of these models is that they are often simple enough to allow for analytic investigation, however, they do not allow the ability to capture chain length dependent behaviours.

Alternatively, discrete population-balance equations, first applied to the degradation of polymers by Simha (1941), can be used to formulate a system of coupled kinetic equations that accounts for all oligomeric intermediates in the reaction, such that the degree of polymerisation of the material determines the size of the equation system. Population-balance equations enable the observation of behaviours that are influenced by chain length and thus obtain time-dependent oligomer profiles. This equation structure provides a more flexible foundation for the kinetics of hemicellulose degradation and thus forms the basis of the model presented in this work.

However, kinetic models alone may not fully actualise the chemistry that is occurring during the pretreatment of substrates with complex structures, such as bagasse or other biomasses. Because of the fibrous nature of these materials, reagents may have a tortuous diffusion pathway and may only be able to make contact with a small proportion of substrate. Likewise, as chains are scised and solubilised and removed from the cell wall by diffusive fluxes, the structure of the substrate changes and the reaction is better able to progress uninhibited. A measure of the accessibility of the substrate is the material porosity. Previous models for hemicellulose or cellulose degradation have included poros-

ity calculations, however these often introduce unknown parameters into the model, or require that the substrate is well defined geometrically (Griggs et al., 2011; Levine et al., 2010; Mittal et al., 2009; Zhou et al., 2009). On the small scale of the bagasse cell wall, the exact spatial distribution and geometric properties of the fibre network cannot be easily understood.

In this work, we have developed a volume-averaged model for acid hydrolysis on a microscopic scale. Volume averaging infers that at any given spatial co-ordinate there exists some fraction of each of the solid materials and some fraction of liquid (initially the acid solution) (Whitaker, 1998). The liquid fraction represents the porosity of the material, which can be modelled using conservation of volume arguments. Therefore, the model accounts for acid-catalysed chain scission using a population balance framework, the structure of which facilitates the solubilisation and diffusion of short-chain oligomers, and selectivity in the formation of degradation products. Solubilisation affects the porosity of the material, which in turn influences the reactivity and ease of diffusion due to the coupled nature of the equation system. Non-dimensionalisation of the model reduces the number of parameters in the system to a few key ratios, thus framing a discussion about the influence of the various parameters on pretreatment effectiveness. Although the modeling work in this paper is phrased around bagasse, the model itself is portable across many lignocellulosic biomass feedstocks.

The intention is for this model not to be used as a predictive tool, but rather as a means of understanding the processes occurring in the cell wall. We will ultimately incorporate this model into a macroscopic model of the acid hydrolysis of a bagasse fibre, which will be designed to be predictive.

Model Development

Consider a one-dimensional cross section of the cell wall ($0 \leq x \leq L$) of a representative bagasse fibre (Figure 1), where the spatial dimension, x, has units of metres. The

cell wall is comprised of a lignocellulosic matrix flooded with an acid solution (H_3O^+), of which the cellulosic fibrils are coated and interlinked by hemicelluloses. These amorphous hemicelluloses can be hydrolysed and removed from the cell wall, allowing enzymes better access to the cellulosic substrate in downstream biofuel processing. Hydrolysed hemicellulose chains leave the system through diffusion out of the cell wall and into the bagasse lumen. Given the one-dimensional nature of the problem, we are assuming that diffusion is defined orthogonal to the cell wall-lumen interface and that diffusion longitudinally within the cell wall is ignored. There is a further macroscopic mathematical problem associated with the transport of hemicellulose chains through the bagasse lumen and into the bulk hydrolysate, however, in this paper we are only concerned with the cell wall kinetics.

[Figure 1 near here (color online)]

There are three key phenomena that need to be considered in modeling the acid hydrolysis of hemicellulose within the cell wall; scission events, size dependent diffusion of hemicellulose chains and the impact that these processes have upon the porosity of the material. Implicit in the model equations are the assumptions

1. all physical processes are isothermal and isobaric;
2. xylan is representative of the hemicellulosic material, since the pentose xylose is typically the primary constituent of hemicellulose in bagasse (Gírio et al., 2010);
3. furfural represents the degradation products of xylose (refer to Figure 2);
4. the fraction of the total volume occupied by cellulose and lignin is unchanged under the conditions of dilute acid hydrolysis;
5. the cell wall is saturated with acid solution such that there are only liquid and solid volume fractions to consider in the model derivation, denoted ϵ_v and ϵ_s, respectively;
6. volume is conserved throughout the hydrolysis process.

The liquid volume fraction, ϵ_v, (i.e. the ratio of liquid or void volume to total volume) is the porosity of the fibrous material.

Since it is not possible to know the exact spatial distribution of all elements within the bagasse cell wall due to its small size and fibrous internal structure, formulating a geometric model is not a viable option at this scale. Consequently, we apply a volume averaging argument as per the methods outlined by Whitaker (1998), such that at any given spatial point both solid and liquid fractions can co-exist. Volume averaging leads to effective concentrations of xylan chains of length i, ϕ_i ($\mathrm{kg\,m^{-3}}$), the effective concentration of furfural, ϕ_F ($\mathrm{kg\ m^{-3}}$), and an effective concentration of acid, ψ_{H^+} ($\mathrm{mol\,m^{-3}}$), defined such that

$$\psi_{H^+} = \epsilon_v C_{H^+}; \quad \phi_F = \epsilon_v \rho_F; \quad \phi_i = \epsilon_v \rho_i \quad i = 1 \ldots m; \quad \phi_i = \epsilon_i \rho_s \quad i = m+1 \ldots N;$$

where ρ_i and ρ_F ($\mathrm{kg\,m^{-3}}$) are the densities of a xylo-oligomer of length i in solution and furfural respectively, ρ_s ($\mathrm{kg\,m^{-3}}$) is the material density of solid xylan, C_{H^+} ($\mathrm{mol\,m^{-3}}$) is the concentration of acid per volume of liquid, m is the chain length at which hemicellulose chains are solubilised to form aqueous oligomers, and N is the maximum chain length of hemicellulose.

[Figure 2 near here]

Figure (2) represents possible reaction pathways for the dilute acid hydrolysis of hemicellulose. These kinetics can be captured using a population balance framework, for which the time evolving concentrations of all chain lengths are explicitly accounted. This provides information about the polydispersity of hemicellulose over time and allows for the inclusion of polymer characteristics (such as solubility) as a function of chain length. Depending upon the position of the hydrolysed bond, the initially monodisperse initial distribution of hemicellulose chains may form similarly insoluble long xylan chains, or oligomers and monomers that have a small enough degree of polymerisation to be solubilised in the acid solution. Dehydration of xylose leads to the degradation product

furfural (Binder et al., 2010).

Different reaction rates are used to distinguish between hydrolysis of solid, k_a ($\mathrm{m^3\,mol^{-1}\,s^{-1}}$), and aqueous, k_b ($\mathrm{m^3\,mol^{-1}\,s^{-1}}$), chains. Likewise, k_d ($\mathrm{m^3\,mol^{-1}\,s^{-1}}$) represents the degradation rate of xylose to produce furfural. Arrhenius kinetics of the form,

$$k = k^0 \exp\left(\frac{-E_a}{RT}\right), \tag{1}$$

are used to formulate the rate parameters. The choice of distinct rate parameters for the solid and solution phase kinetics is motivated by the influence of solvation on the enthalpy and/or entropy components of the Gibbs free energy of the reaction (Henriksen and Hansen, 2008). The transition between the solid and liquid fraction due to solubilisation must be accounted for in the porosity calculations (described later as per Equation 14 and associated discussion).

In addition to the kinetic events described in Figure (2) the model accounts for the diffusion of all aqueous species including oligomeric xylan (chains of length $i = 2 \dots m$), xylose ($i = 1$) and furfural. The resultant model system is therefore

$$\frac{\partial \phi_F}{\partial t} = \underbrace{k_d \psi_{H^+} \phi_1}_{\text{Formation}} + \underbrace{\frac{\partial}{\partial x}\left(D^F_{\text{eff}} \frac{\partial \phi_F}{\partial x}\right)}_{\text{Diffusion}}, \tag{2}$$

$$\frac{\partial \phi_1}{\partial t} = \underbrace{-k_d \psi_{H^+} \phi_1}_{\text{Degradation}} + \underbrace{2k_a \psi_{H^+} \sum_{j=m+1}^{N} \Omega_{1,j-1} \phi_j}_{\text{Formation from solid chains}} + \underbrace{2k_b \psi_{H^+} \sum_{j=2}^{m} \Omega_{1,j-1} \phi_j}_{\text{Formation from aqueous chains}} + \underbrace{\frac{\partial}{\partial x}\left(D_{\text{eff}} \frac{\partial}{\partial x} \phi_1\right)}_{\text{Diffusion}}, \tag{3}$$

$$\frac{\partial \phi_i}{\partial t} = \underbrace{-k_b \psi_{H^+} \phi_i}_{\text{Scission}} + \underbrace{2k_a \psi_{H^+} \sum_{j=m+1}^{N} \Omega_{i,j-i} \phi_j}_{\text{Formation from solid chains}} + \underbrace{2k_b \psi_{H^+} \sum_{j=i+1}^{m} \Omega_{i,j-i} \phi_j}_{\text{Formation from aqueous chains}} + \underbrace{\frac{\partial}{\partial x}\left(D_{\text{eff}} \frac{\partial}{\partial x} \phi_i \right)}_{\text{Diffusion}},$$

$$(i = 2, 3, \ldots, m-1, m) \quad (4)$$

and

$$\frac{\partial \phi_i}{\partial t} = \underbrace{-k_a \psi_{H^+} \phi_i}_{\text{scission}} + \underbrace{2k_a \psi_{H^+} \sum_{j=i+1}^{N} \Omega_{i,j-i} \phi_j}_{\text{Formation from solid chains}}, \quad (i = m+1, m+2, \ldots, N-1, N) \quad (5)$$

where Equations (2) through (5) describe the time rate of change of the concentrations of furfural, xylose, aqueous oligomers and xylan respectively. The summation terms are indicative of the many possible ways a polymer chain can be formed from all longer chain lengths. Here $\Omega_{i,j-i}$ is the breakage kernel and D_{eff} ($\text{m}^2\,\text{s}^{-1}$) represents an effective diffusion coefficient used to account for the tortuous nature of the bagasse cell wall. The breakage kernel is given by

$$\Omega_{i,j-i} = \omega_{i,j-i} m_{f_i}, \qquad i = 1, 2, \ldots, j-1\,, \quad j = 2, 3, \ldots, N \quad (6)$$

where $\omega_{i,j-i}$ ($0 \leq \omega_{i,j-i} \leq 1$) is the probability that a chain of length j will produce a chain of length i and a chain of length $j-i$ (in a binary breakage environment), and m_{f_i} is the proportion of mass that such a breakage would contribute to the i^{th} class. More specifically, the mass fraction, m_{f_i} is the ratio of the chain length that is being produced, and the chain length that is being scised, namely,

$$m_{f_i} = \frac{i}{j}, \qquad i = 1, 2, \ldots, j-1\,, \quad j = 2, 3, \ldots, N. \quad (7)$$

We assume that there are no preferential scission sites across the xylan chain, and thus each of the $j-1$ bond sites has an equal probability, namely,

$$\omega_{i,j-i} = \frac{1}{j-1}, \qquad i = 1, 2, \ldots, j-1\,, \quad j = 2, 3, \ldots, N \tag{8}$$

of being scised from either end of the symmetric hemicellulose chain. When $i \neq j/2$, any particular chain length can be achieved by executing a scission event from the left or right hand end of a chain. Consequently, each of the scission terms in Equations (2) to (5), has a coefficient of two to account for both the left and right hand scission events. Conversely, if $i = j/2$ (i.e. the chain is being scised into two exactly equal parts), the probability of scission is no longer increased as there is only one possible bond that can be scised to produce this result. However, such an event results in twice the mass of a single chain length being produced. We note that according to our definition of m_{f_i} in Equation (7), when $i = j/2$, then $m_{f_i} = 1/2$. In this case the coefficient of two in Equations (2) to (5) is absorbed by the mass fraction term in the breakage kernel, such that $2m_{f_i} = (2)(1/2) = 1$, as required. It is important to note that the formulation of the breakage kernel given in Equation (6), maintains conservation of mass in a diffusionless system.

The effective diffusion coefficient is dependent upon the porosity of the material, such that

$$D_{\text{eff}}(i, \epsilon_v) = \epsilon_v^3 D_\infty(i), \qquad (i = F, 1, 2, \ldots, m) \tag{9}$$

where $D_\infty(i)$ ($\mathrm{m^2\,s^{-1}}$) is the chain length dependent diffusion coefficient of the hemicellulose material outside of the tortuous cell wall environment. The cubic dependence on porosity was informed by the random porous cluster modification to the diffusion coefficient used by Lee and Park (2007) to describe mass transport in biofilms. Since polymers can coil in solution, we make the assumption that the solubilised chains are approximately spherical, with hydrodynamic radius R_e (m). We are thus able to use a Stokes-Einstein approximation to the diffusion coefficient (Cussler, 1997) to represent $D_\infty(i)$, namely,

$$D_\infty(i) = \frac{k_B T}{6\pi\eta R_e}, \quad R_e = 0.676\, l\sqrt{i} \tag{10}$$

where k_B (m^2 kg s^{-2} K^{-1}) is Boltzmann's constant, η (kg m^{-1} s^{-1}) is the dynamic viscosity of the acid solution, and l (m) is the length of a single xylose monomer.

Dirichlet boundary conditions,

$$\phi_i(0,t) = \phi_i(L,t) = 0 \tag{11}$$

are imposed upon the system to represent an advective flux in the plant lumen, such that any hemicellulose chains that reach the cell wall boundary are instantly removed by the advective flow. This is a simplifying assumption that will be examined in detail in further work by the authors on the development of a coupled macroscopic-microscopic model of transport in bagasse elements.

It must be noted that the reaction scheme given in Figure (2) and embodied in Equations (2) to (5) does not take into consideration two separate 'hard to hydrolyse' and 'easy to hydrolyse' xylan fractions, popularised in the literature by Kobayashi and Sakai (1956). We acknowledge that the complicated and non-uniform structure of hemicellulose is likely to influence the reaction kinetics of hydrolysis, however, the concept of two separate hard and easy to hydrolyse fractions is not easily incorporated into the population balance equations in a physically motivated way.

The concept of two separate substrates creates a large number of additional equations to be solved at each timestep, and introduces the need to define difficulty of hydrolysis by some physical characteristic(s) of the chains that can be modelled as an additional variable. After each scission event, the products would need to be reclassified as easy or hard to hydrolyse based on the time-evolving status of these defining characteristics. Until a mechanism is developed to characterise the easy and hard to hydrolyse hemicellulose fractions, it remains beyond the scope of this work to adopt the kinetic pathway of Kobayashi and Sakai.

Cell Wall Porosity

Using SEM imaging, Zhang et al. (2011) observed a change in the structure of sourghum bagasse after acid hydrolysis. In particular, they observed that cellulose in the bagasse became more accessible due to the appearance of microholes in the material. Our model attempts to quantify such changes, by explicitly monitoring the time evolving porosity of the bagasse cell wall substrate caused by the solubilisation and subsequent diffusion of hemicelluloses throughout the cell wall. The porosity of the domain changes since the ratio of solid to liquid materials in the system is not constant.

Conservation of volume requires that

$$\epsilon_s + \epsilon_v = 1, \tag{12}$$

where the solid volume fraction, ϵ_s, accounts for the volume of cell wall occupied by cellulose, lignin and solid hemicelluloses, and the void fraction, ϵ_v, is comprised of the acid solution and any solubilised hemicellulose chains (i.e. chains for which $i < m$). We make the simplifying assumption that only hemicellulose reacts with the acid solution, and that cellulose and lignin maintain a constant combined volume fraction, $\hat{F}$. Therefore, the solid volume fraction can be described by the equation

$$\epsilon_s = \hat{F} + \sum_{i=m+1}^{N} \epsilon_i, \tag{13}$$

since it is only chains of length greater than m that contribute to the solid volume fraction. It follows that substitution of Equation (13) into Equation (12) dictates that the porosity equation is of the form

$$\epsilon_v = 1 - \left(\hat{F} + \sum_{i=m+1}^{N} \epsilon_i \right). \tag{14}$$

Consequently, we have arrived at a coupled system of $N+2$ equations (partial differential equations (2) to (5) and algebraic equation (14)), to describe hemicellulose degradation, furfural production and porosity evolution, governed by Dirichlet boundary conditions,

(Equation 11), and the monodisperse initial condition

$$\phi_i(x,0) \;=\; \phi_N(x) \;= C_N^0. \tag{15}$$

A compilation of parameter values and their sources is provided in Table (I). Many of these parameters were obtained directly from the literature, however there are some that require further explanation. Some parameters such as the degree of polymerisation of hemicellulose can not be reduced to a single value since the material is naturally polydisperse. Hence the reported value of N was chosen to be within the measured range of the DP of hemicellulose, such that the running time of the numerical simulation remained feasible. The oligomer diffusion coefficients were calculated using the Stoke's Einstein formulation (Equation 10), and the diffusion coefficient of chains of length m in particular was selected as a scaling factor for the non-dimensionalisation of the model equations (discussed in the following section) to represent the slowest diffusing chains. The acid concentration C_{H^+} given in the table has been converted to SI units from a reported acid concentration of 4 wt% (Lavarack et al., 2000) in order to be consistent with the second order rate kinetics used in the formulation of the reaction terms. The acid concentration was assumed to remain constant, since the transport time for acid into the cell wall is fast compared to the reaction and transport of oligomers. This is because the ionic radius of a hydrogen ion is approximately an order of magnitude smaller than the smallest oligomer chain, i.e. a xylose monomer (Aylward and Findlay, 2008; Weng et al., 2009). Consequently, due to the inverse dependency upon hydrodynamic radius in the Stokes-Einstein formulation for the diffusion coefficient, we would expect hydrogen ions to diffuse approximately one order of magnitude faster (Cussler, 1997).

Some of the parameters were estimated, such as the intial condition and the volume fraction of cellulose and lignin. These parameters were chosen to represent a cell wall with very little porous space, hence the volume fraction of cellulose, lignin and hemicellulose were estimated to initially sum to 95% of the total cell wall volume. There had to be some non-zero acid concentration initially for the reaction to take place. The choice of $\hat{F}$

was intended to approximate the relative amounts of cellulose, lignin and hemicellulose as a hydrated volume fraction, from available data of the composition of dried bagasse (O'Hara et al., 2011).

[Table I near here]

Numerical Methods

Non-dimensionalisation of the model system can be achieved by scaling each of the dimensioned variables, such that

$$\bar{\phi_F} = \frac{\phi_F}{\rho_s}, \quad \bar{\phi_i} = \frac{\phi_i}{\rho_s}, \quad \bar{x} = \frac{x}{L}, \quad \bar{D}_\infty = \frac{D_\infty}{D^*_\infty}, \quad \bar{t} = k_a C_{H^+} t.$$

Applying these scalings to Equations (2) to (5) and (11), we obtain the following dimensionless equation system:

$$\frac{\partial \bar{\phi}_F}{\partial \bar{t}} = \delta_{1_F} \epsilon_v \bar{\phi}_1 + \delta_{2_F} \frac{\partial}{\partial \bar{x}} \left(\epsilon_v^3 \frac{\partial \bar{\phi}_F}{\partial \bar{x}} \right) \tag{16}$$

$$\frac{\partial \bar{\phi}_i}{\partial \bar{t}} = -\delta_{1_F} \epsilon_v \bar{\phi}_i + 2\epsilon_v \sum_{j=m+1}^{N} \Omega_{i,j-i} \epsilon_j + 2\delta_1 \epsilon_v \sum_{j=i+1}^{m} \Omega_{i,j-i} \bar{\phi}_j + \delta_2 \frac{\partial}{\partial \bar{x}} \left(\epsilon_v^3 \bar{D}_\infty \frac{\partial}{\partial \bar{x}} \bar{\phi}_i \right), \quad (i = 1) \tag{17}$$

$$\frac{\partial \bar{\phi}_i}{\partial \bar{t}} = -\delta_1 \epsilon_v \bar{\phi}_i + 2\epsilon_v \sum_{j=m+1}^{N} \Omega_{i,j-i} \epsilon_j + 2\delta_1 \epsilon_v \sum_{j=i+1}^{m} \Omega_{i,j-i} \bar{\phi}_j + \delta_2 \frac{\partial}{\partial \bar{x}} \left(\epsilon_v^3 \bar{D}_\infty \frac{\partial}{\partial \bar{x}} \bar{\phi}_i \right),$$

$$(i = 2, 3, \ldots, m-1, m) \tag{18}$$

$$\frac{\partial \epsilon_i}{\partial \bar{t}} \quad = \quad -\epsilon_v \epsilon_i \; + \; 2\epsilon_v \sum_{j=i+1}^{N} \Omega_{i,j-i} \epsilon_j, \quad (i \; = \; m \; + \; 1, m \; + \; 2, \ldots, N \; - \; 1, N) \quad (19)$$

$$\epsilon_v = 1 - \left(\hat{F} + \sum_{i=m+1}^{N} \epsilon_i \right), \tag{14}$$

where the number of parameters has been reduced to four dimensionless ratios, namely,

$$\delta_1 = \frac{k_b}{k_a}, \qquad \delta_{1_F} = \frac{k_d}{k_a}, \qquad \delta_2 = \frac{D^*_\infty}{L^2 k_a C_{H^+}}, \qquad \delta_{2_F} = \frac{D^{F^*}_\infty}{L^2 k_a C_{H^+}}.$$

The parameter groupings δ_1 and δ_{1_F} represent timescale ratios of the rate of aqueous chain scission and the rate of degradation product formation, to the rate of solid hemicellulose chain scission respectively. The parameters δ_2 and δ_{2_F} represent ratios of the timescale of polymer scission to the timescale of hemicellulose diffusion and the timescale of furfural diffusion respectively.

The magnitude of δ_1, δ_{1_F}, δ_2 and δ_{2_F} will determine the relative influence of scission and diffusion on the system and allows us to investigate the sensitivity of our model to these behaviours using a reduced set of unknown parameters. These parameters are described as 'unknown' due to the difficulty of measuring the reaction rate and diffusion parameters and consequently because of the lack of agreement on these values in the literature (as discussed in Sensitivity to δ_{1_F}). Unless otherwise indicated, the standard parameter values in Table (I) form the basis for the numerical simulation.

The model equations are formed in terms of three variables: chain length, i, space, x, and time, t. Chain length is already incorporated into the model as a discrete variable. The numerics were facilitated through the application of a vertex-centered finite volume discretisation across the spatial terms in order to reduce the system of partial differential equations to a system of ordinary differential equations in time (Patankar, 1980). Using the MATLAB interface to SUNDIALS (Hindmarsh et al., 2005), the IDA solver

was used to implement the discretised differential algebraic equation system over 51 uniformly spaced spatial nodes. The running time of each implementation of the model was substantial, of the order of several hours duration. The authors note that, although the banded structure of the Jacobian was utilised, the code was not optimised for fast performance. Optimisation of the implementation of the model equations is a potential avenue for future investigation.

Results and Discussion

For all of the results presented in this article, the yield of oligomers of chain length i, Y_i, was calculated on a mass basis, such that

$$Y_i = \frac{\sum\limits_{\hat{x}} \text{mass}_{i_{\text{final}}}}{\sum\limits_{\hat{x}} \text{mass}_{N_{\text{initial}}}} = \frac{\sum\limits_{\hat{x}} \bar{\rho}_i}{\sum\limits_{\hat{x}} \bar{\rho}_N}. \tag{20}$$

Here only the initial mass of chains of length N were considered due to the monodisperse nature of the initial condition. Throughout this document, yields are presented as mass fractions rather than percentages.

As we have seen, the non-dimensionalisation of the model equations introduced four dimensionless ratios, δ_1, δ_{1_F}, δ_2 and δ_{2_F}, consisting of reaction rates and diffusion coefficients. These parameters are difficult to measure experimentally, hence the dimensionless ratios are susceptible to inaccuracy. This is a concern, since the validity of the yields predicted by the model is influenced by the accuracy of these parameter values.

Figure (3) demonstrates the sensitivity of the model equations to the dimensionless ratios δ_1, δ_{1_F}, δ_2 and δ_{2_F}. In this figure, variations in the maximum xylose yield were recorded as a result of changing the dimensionless ratios by $\pm 5\%$, from unity, in turn. Figure (3) demonstrates that parameters δ_1, δ_{1_F} and δ_2 can significantly influence the monomer yield, while δ_{2_F} has limited impact in this instance. This is understandable, since δ_{2_F} is only apparent in the differential equation concerned with the time rate of change of

furfural concentration (Equation 16), and thus has no direct impact upon the yield of the xylose and hemicellulose products of key concern in this work. Consequently, in the proceeding discussion we will consider in detail the influence that parameters δ_1, δ_{1_F} and δ_2 exercise upon the yield of xylose oligomers resulting from dilute acid pretreatment.

[Figure 3 near here]

Sensitivity to δ_{1_F}

As noted earlier, the parameter δ_{1_F} is representative of the relative rates of furfural formation and solid hemicellulose scission in a diffusionless system (i.e. $\delta_2, \delta_{2_F} = 0$). Figure (4) shows the influence that δ_{1_F} imparts on the yield of monomer obtained before xylose is dehydrated to form furfural.

It must be noted that, although the timescale of hydrolysis may seem fast in Figure (4), (and Figures (7) and (8) to follow), these results are representative of a microscopic domain and hence we would expect shorter reaction times that those observed at a reactor level. Additionally, the choice of the dimensionless ratios $\delta_1, \delta_{1_F}, \delta_2$ and δ_{2_F} may be varied to alter the speed of the hydrolysis process, and hence in the absence of a complete multi-scale model the timescale of the microscopic reaction as a lone quantity is not significant to the interpreation of the results.

[Figure 4 near here]

By fixing $\delta_1 = 1$, it can be seen that decreasing δ_{1_F} improves the yield of monomer obtained because this favours the rate of chain scission over furfural formation. If we anticipate any appreciable yield of xylose over furfural, we might approximate the parameter space of δ_{1_F} to be $\delta_{1_F} \leq 1$. Experimental data of the comparative amounts of xylose and furfural in the pretreatment hydrolysate can be used to narrow the potential parameter space under various ambient conditions.

Because of the Arrhenius kinetics used to formulate the rate constants, we can identify a relationship between δ_{1_F} and the operating temperature of the reaction vessel, such that

$$\delta_{1_F} = \frac{k_d}{k_a} = \beta_{1_F} \exp\left(\frac{\gamma_{1_F}}{\mathrm{RT}}\right), \tag{21}$$

where

$$\beta_{1_F} = \frac{k_d^0}{k_a^0}, \tag{22}$$

and

$$\gamma_{1_F} = E_{a_a} - E_{a_d}. \tag{23}$$

In the literature there appears to be some inconsistency regarding the temperature dependence of δ_{1_F}. Figure (5) presents the relationship between δ_{1_F} and temperature for different sets of biomass acid pretreatment rate parameters taken from the literature as collated by Liu et al. (2012) (Table II). Each of the three parameter sets predicts different temperature dependent behaviour of δ_{1_F}. Parameter set one suggests that there is very little change in δ_{1_F} as the temperature in the reaction vessel fluctuates, whereas parameter sets two and three indicate opposite trends, with δ_{1_F} increasing and decreasing with temperature, respectively. Some discrepancy may be due to variations in the structure of the different materials, however the contrast evident in Figure (5) is quite extreme given that each of the feedstocks share a similar lignocellulosic composition (O'Hara et al., 2011). Any variations in experimental conditions such as temperature or acid concentration should not influence the rate parameters, as these are not constant in their formulation, but rather variables that should be able to be altered without loss of accuracy (if the rate parameters themselves are accurate).

[Figure 5 near here]

[Table II near here]

These contradictory behaviours can be explained by considering the inverse temperature relationship in the exponent of the Arrhenius equation. Equation (21) identifies the two

key relationships that govern the shape of δ_{1_F}; the ratio of pre-exponential factors β_{1_F}, which determines the magnitude and high temperature limit of δ_{1_F}, and the difference of activation energies for the scission and degradation reactions γ_{1_F}, which determines if δ_{1_F} will be an increasing or decreasing function (as demonstrated for the general case in Figure 6). The sign of γ therefore also determines whether β is a local minima or maxima in the high temperature limit. Figure (5) demonstrates the sensitivity of the δ_{1_F} parameter to discrepancies in these pre-exponential and the activation energy parameters. These kinetic parameters are difficult to measure, and are often determined through a data fitting process. However, depending on the algorithm used and number of free parameters allowed in the fitting process, the parameter values obtained can vary significantly. Also, parameters that return similar results when fit to a particular set of data, such as a timeseries of yield curves, may not demonstrate the same congruence when considered in another context (such as temperature dependence in Figure 5). When parameters are determined through a data fitting process, physicality of the system is not always explicitly accounted for.

[Figure 6 near here]

Sensitivity to δ_1

The parameter δ_1 is the ratio of the rates of hydrolysis for aqueous and solid hemicellulose. Figure (7) shows the yield curves for soluble oligomers up to five monomer units in length in a diffusionless system (i.e. δ_2, $\delta_{2_F} = 0$), and their dependence on the parameter δ_1 (for $\delta_{1_F} = 1$). If δ_1 is unity, it represents equal rates of acid hydrolysed scission of the solid and aqueous hemicellulose. A value of δ_1 less than one indicates that scission of solid hemicellulose is faster, and conversely δ_1 greater than one suggests faster hydrolysis of aqueous chains. We can see that varying the δ_1 parameter affects the oligomer profiles observed in the hydrolysate. If the rate of scission of aqueous chains is too fast (Figure 7c), all small chain oligomers become monomers so quickly that we do not see a distinct yield of oligomers in the microscale hydrolysate. Although the reaction conditions will

influence the oligomer profile of the reaction, we would expect to observe some oligomers in the hydrolysate in congruence with the experimental results of Li et al. (2003) and Yang and Wyman (2008a).

[Figure 7 near here (color online).]

Yang and Wyman (2008a) show that at 200°C the macroscale hydrolysate from the acid-free hydrolysis of corn stover contains aqueous oligomers of up to thirty monomer units in length, some in substatial quantities. We would expect this result to be magnified on the microscale, as the microscale oligomers have yet to be further exposed to the acid (and thus more scission) in the plant lumen before entering the bulk hydrolysate. Such an observation is more consistent with the yield curves in Figures (7a) and (7b). Consequently, we might expect an approximate parameter space of $\delta_1 \leq 1$, where the solubilised hemicellulose is harder to hydrolyse than its solid counterpart. Although we may intuitively expect there to be greater opportunities for molecular collisions in the solution phase, the rate of hydrolysis of aqueous hemicellulose may be affected by solute-solvent interactions and any desolvation energies affecting the free energy of activation, $\Delta G^{\ddagger}$ (Henriksen and Hansen, 2008).

Sensitivity to δ_2

The parameter δ_2 represents the ratio of the rate of diffusion of chains of length m and the rate of hemicellulose scission.

Figure (8) shows changes in yield as a result of varying δ_2, neglecting degradation products (i.e. $\delta_{1_F} = 0$ and $\delta_{2_F} = 0$) and setting $\delta_1 = 1$ for simplicity. The absence of degradation products implies that low yields of xylose in Figure (8) are equivalent to high yields of oligomers leaving the cell wall. Changing δ_2 affects the predicted oligomer profiles because slow diffusion allows for all chains to be hydrolysed to monomers before they are removed from the cell wall environment. Alternatively, fast diffusion means that longer chains are removed before scission can occur.

[Figure 8 near here (color online).]

A choice of δ_2 where diffusion is favoured over scission seems reasonable given that hemicellulose oligomers are measured in the macroscale hydrolysate (Yang and Wyman, 2008a), hence we may expect an approximate parameter space of $\delta_2 \geq 0.01$.

Constrained Fitting

We have observed that variations in the magnitude of the dimensionless ratios δ_1, δ_{1_F} and δ_2 can significantly influence the predicted outcomes of the mathematical model, and hence the validity of the model results can be compromised by inaccuracies in the input parameters. Unfortunately, due to the difficulty in directly measuring kinetic parameters, data fitting procedures are often used to elucidate key model parameters. As discussed for the case of δ_{1_F}, this can lead to incongruent parameter calculations across different experimental studies.

A potential first step to incorporating physicality into the fit of these parameters may be to introduce a constrained fitting process. Introducing physical constraints into the fitting process reduces the number of potential parameter choices and can ensure the resultant parameters satisfy multiple experimentally motivated criteria.

Although the model presented in this work is formulated on the microscopic scale (for which experimental data cannot be obtained), we believe that macroscopic data can be used to infer information on the microscale, as the microscale is ultimately the source of any chemical information recorded in the bulk hydrolysate and hence the two are intimately related. Consequently, we have been able to qualitatively estimate approximate parameter spaces for the dimensionless ratios δ_1, δ_{1_F} and δ_2 by comparing the theoretical yield curves with published macroscale experimental observations. These limitations on the parameter space provide constraints that could be implemented as part of a multi-scale fitting process. Likewise, by experimentally investigating the relationship between the dimensionless ratios and temperature, further limiting constraints may be obtained

regarding the β and γ parameters that govern the ratios of Arrhenius functions, such as δ_{1_F} and δ_1.

No experiments have yet been conducted by the authors to further quantify these constraints, since no data fitting techniques can be applied until a macroscopic scale is coupled to the current model equations. However, it is possible that application of a constrained parameter fit on a multi-scale model would result in less discrepancy between the parameters determined by different experimental studies.

Conclusions

In this work a mathematical model of the acid hydrolysis, degradation and diffusion of hemicellulose chains within the cell wall of bagasse has been developed. This was achieved using a population-balance approach to describe the scission events, with careful consideration given to the breakage kernel to ensure conservation of mass. Using a conservation of volume argument, the model is able to account for the time-evolution of the material porosity, thus accounting for solubilisation and diffusion of short chain oligomers. The result of the model is a time-series of oligomer profiles than can be pinpointed at particular spatial locations within the cell wall, or summed over the total area to produce the yield curves discussed throughout the paper.

Although we are unable to compare our results directly with experimental data due to the size scale of interest, non-dimensionalisation reduces the parameter space of the equation system to four key ratios. A sensitivity analysis of these ratios allows us to infer constraints on our unknown parameter values, and provides a foundation for deeper consideration of the relationship between the model parameters and the fundamental thermodynamic processes that are occurring during acid pretreatment. As a result, we can determine that careful consideration is required when obtaining parameter values through conventional data fitting and that the generality and accuracy of such models may be improved if parameters are obtained with a consciousness of the underlying

chemistry and physics of acid pretreatment. Here we have developed the first component of a multiscale mathematical model of sugarcane bagasse that can be used to address these parameter fitting issues.

Acknowledgements

Computational resources and services used in this work were provided by the HPC and Research Support Group and Mr Steven Dargaville, Queensland University of Technology, Brisbane, Australia.

Nomenclature

Roman

C_{H^+}	(mol m^{-3})	Concentration of acid in the solution
D^*_∞	(m^2 s^{-1})	Bulk diffusion coefficient of hemicellulose chains of length m
D^F_∞	(m^2 s^{-1})	Bulk diffusion coefficient of furfural
D_{eff}	(m^2 s^{-1})	Effective diffusion coefficient of hemicellulose
D^F_{eff}	(m^2 s^{-1})	Effective diffusion coefficient of Furfural
E_a	J mol^{-1}	Activation energy
$\hat{F}$	-	Volume fraction of cellulose and lignin
k_a	(m^3 mol^{-1} s^{-1})	Rate of scission of solid hemicellulose
k_b	(m^3 mol^{-1} s^{-1})	Rate of scission of aqueous hemicellulose
k_B	(m^2 kg s^{-2} K^{-1})	Boltzmann constant
k_d	(m^3 mol^{-1} s^{-1})	Rate of degradation of xylose to produce furfural
l	(m)	Length of a xylose monomer
L	(m)	Width of the cell wall
m	-	Chain length at which oligomers become soluble
N	-	Degree of polymerisation of hemicellulose (max. chain length)

R	(J mol^{-1} K^{-1})	Gas constant
t	(s)	Time
T	(K)	Temperature
x	(m)	Spatial variable

Greek

δ	-	Dimensionless ratio
ϵ_s	-	Solid volume fraction
ϵ_v	-	Void volume fraction (porosity)
η	(kg s^{-1} m^{-1})	Viscosity of acid
ρ_F	(kg m^{-3})	Density of furfural per volume of solution
ρ_i	(kg m^{-3})	Density of hemicellulose chains of length $i \leq m$ per volume of solution
ρ_s	(kg m^{-3})	Density of solid hemicellulose chains
ϕ_F	(kg m^{-3})	Effective density of furfural
ϕ_i	(kg m^{-3})	Effective density of chains of length $i \leq m$
ψ_{H^+}	(mol m^{-3})	Effective concentration of acid
$\Omega_{i,j-i}$	-	Breakage kernel

Subscripts and Superscripts

- 0 - Pre-exponential component of rate constant
- i - Chain length counter

References

Albersheim, P., Darvill, A., Roberts, K., Sederoff, R., and Staehelin, A. (2011). *Plant Cell Walls*. Garland Science, New York.

Australian Government (2004). *The Biology and Ecology of Sugarcane (Saccharum* spp hybrids) in Australia. Department of Health and Ageing, Office of the Gene Technology Regulator.

Aylward, G. and Findlay, T. (2008). *SI Chemical Data*. John Wiley & Sons, Milton, 6th edition.

Binder, J. B., Blank, J. J., Cefali, A. V., and Raines, R. T. (2010). Synthesis of furfural from xylose and xylan. *ChemSusChem*, 3:1268–1272.

Cussler, E. (1997). *Diffusion: mass transfer in fluid systems*. Cambridge University Press, Cambridge, 2nd edition.

Gírio, F., Fonseca, C., Carvalheiro, F., Duarte, L., Marques, S., and Bogel-Łukasik, R. (2010). Hemicelluloses for fuel ethanol: A review. *Bioresour. Technol.*, 101(13):4775 – 4800.

Griggs, A. J., Stickel, J. J., and Lischeske, J. J. (2011). A mechanistic model for enzymatic saccharification of cellulose using continuous distribution kinetics I: Depolymerization by EG_I and CBH_I. *Biotechnol. Bioeng.*, 109:665–675.

Henriksen, N. E. and Hansen, F. Y. (2008). *Theories of Molecular Reaction Dynamics*. Oxford University Press, Oxford, 1st edition.

Hindmarsh, A., Brown, P., Grant, K., Lee, S., Serban, R., Shumaker, D., and Woodward, C. (2005). SUNDIAL suite of nonlinear differential/algebraic equation solvers. *ACM Transactions on Mathematical Software*, 31:363–396.

Jacobsen, S. E. and Wyman, C. E. (2000). Cellulose and hemicellulose hydrolysis models for application to current and novel pretreatment processes. *Appl. Biochem. Biotechnol.*, 84-86:81–96.

Kobayashi, T. and Sakai, Y. (1956). Hydrolysis rate of pentosan of hardwood in dilute sulfuric acid. *Bull. Agr. Chem. Soc. Japan*, 20:1–7.

Lavarack, B., Griffin, G., and Rodman, D. (2000). Measured kinetics of the acid-catalysed hydrolysis of sugarcane bagasse to produce xylose. *Catal. Today*, 63:257–265.

Lavarack, B., Griffin, G., and Rodman, D. (2002). The acid hydrolysis of sugarcane bagasse hemicellulose to produce xylose, arabinose, glucose and other products. *Biomass Bioenergy*, 23:367–380.

Lee, M. W. and Park, J. M. (2007). One-dimensional mixed-culture biofilm model considering different space occupancies of particulate components. *Water Research*, 41:4317–4328.

Levine, S. E., Fox, J. M., Blanch, H. W., and Clark, D. S. (2010). A mechanistic model of the enzymatic hydrolysis of cellulose. *Biotechnol. Bioeng.*, 107:37–51.

Li, X., Converse, A. O., and Wyman, C. E. (2003). Characterization of molecular weight distribution of oligomers from autocatalyzed batch hydrolysis of xylan. *Appl. Biochem. Biotechnol.*, 105-108:515–522.

Liu, X., Lu, M., Ai, N., Yu, F., and Ji, J. (2012). Kinetic model analysis of dilute sulfuric acid-catalyzed hemicellulose hydrolysis in sweet sorghum bagasse for xylose production. *Ind. Crops Prod.*, 38:81–86.

Mittal, A., Chatterjee, S. G., Scott, G. M., and Amidon, T. E. (2009). Modeling xylan solubilization during autohydrolysis of sugar maple and aspen wood chips: Reaction kinetics and mass transfer. *Chem. Eng. Sci.*, 64:3031–3041.

Nigam, P. S. and Singh, A. (2011). Production of liquid biofuels from renewable resources. *Prog. Energy Combust. Sci.*, 37:52–68.

O'Hara, I. M., Zhang, Z., Doherty, W. O., and Fellows, C. M. (2011). Lignocellulosics as a renewable feedstock for chemicalindustry: Chemical hydrolysis and pretreatment processes. In Sanghi, R. and Singh, V., editors, *Green Chemistry for Environmental Remediation*, pages 505–560. John Wiley & Sons, New Jersey.

Olsson, L., Jorgensen, H., Krogh, K. B. R., and Roca, C. (2005). Bioethanol production from lignocellulosic material. In Dumitriu, S., editor, *Polysaccharides: Structural diversity and functional versatility*, pages 957–993. Marcel Dekker, New York, 2nd edition.

Patankar, S. V. (1980). *Numerical Heat Transfer And Fluid Flow*. Taylor & Francis, 1st edition.

Qiang, J., Hongman, Z., Li, S., Liang, Q., and He, H. (2011). Kinetic characterization for hemicellulose hydrolysis of corn stover in a dilute acid cycle spray flow-through reactor at moderate conditions. *Biomass Bioenergy*, 35:4158–4164.

Ressel, J. B. (2007). Wood anatomy - an introduction. In Perré, P., editor, *Fundamentals of Wood Drying*, page 366. A.R.BO.LOR., Nancy.

Saeman, J. F. (1945). Kinetics of wood saccharification, hydrolysis of cellulose and decomposition of sugars in dilute acid at high temperature. *Ind. Eng. Chem.*, 37:42–52.

Scheller, H. V. and Ulvskov, P. (2010). Hemicelluloses. *Annu. Rev. Plant Biol.*, 61:263–289.

Schramke, J. A., Murphy, S. F., Doucette, W. J., and Hintze, W. D. (1999). Prediction of aqueous diffusion coefficients for organic compounds at 25°C. *Chemosphere*, 38:2381–2406.

Simha, R. (1941). Kinetics of degradation and size distribution of long chain polymers. *J. Appl. Phys.*, 12:569–578.

Weng, Y.-H., Wei, H.-J., Tsai, T.-Y., Chen, W.-H., Wei, T.-Y., Hwang, W.-S., Wang, C.-P., and Hwang, C.-P. (2009). Separation of acetic acid from xylose by nanofiltration. *Sep. Purif. Technol.*, 67:95–102.

Whitaker, S. (1998). Coupled transport in multiphase systems: A theory of drying. *Adv. Heat Transfer*, 31:1–104.

Wyman, C., Decker, S., Himmel, M., Brady, J., Skopec, C., and Viikari, L. (2004). Hydrolysis of cellulose and hemicellulose. In Dumitriu, S., editor, *Polysaccharides: Structural Diversity and Functional Versatility*, pages 995–1033. Marcel Dekker, New York, 2nd edition.

Yang, B. and Wyman, C. E. (2008a). Characterization of the degree of polymerisation of xylooligomers produced by flowthrough hydrolysis of pure xylan and corn stover with water. *Bioresour. Technol.*, 99:5756–5762.

Yang, B. and Wyman, C. E. (2008b). Pretreatment: the key to unlocking low-cost celluosic ethanol. *Biofuels, Bioprod. Biorefin.*, 2:26–40.

Zhang, J., Ma, X., Yu, J., Zhang, X., and Tan, T. (2011). The effects of four different pretreatments on enzymatic hydrolysis of sweet sorghum bagasse. *Bioresour. Technol.*, 102:4585–4589.

Zhou, W., Schuttler, H.-B., Hao, Z., and Xu, Y. (2009). Cellulose hydrolysis in evolving substrate morphologies I: A general modeling formalism. *Biotechnol. Bioeng.*, 104:261–274.

List of Tables

Parameter	Meaning	Value	Ref
C_H^+	Acid concentration	$444\ \mathrm{mol\,m^{-3}}$	(Lavarack et al., 2000)
L	Length of the cell wall	1×10^{-6} m	(Ressel, 2007)
D_∞^*	Bulk diffusivity of chains of length m	1.07×10^{-10} $\mathrm{m^2\ s^{-1}}$	(Cussler, 1997)
D_∞^F	Bulk diffusivity of furfural	1.12×10^{-9} $\mathrm{m^2\ s^{-1}}$	(Schramke et al., 1999)
$\hat{F}$	Volume fraction of cellulose and lignin	0.65	
N	Degree of polymerisation of hemicelluloses	100	(O'Hara et al., 2011)
m	Soluble chain length threshhold of hemicellulose	15	(Yang and Wyman, 2008a); Novozymes, 2012[†]
k_B	Boltzmann constant	1.38×10^{-23} $\mathrm{m^2\,kg\,s^{-2}\,K^{-1}}$	(Aylward and Findlay, 2008)
l	Length of a single monomer	0.65×10^{-9} m	(Weng et al., 2009)
C_N^0	Initial dimensionless concentration of chains of length N	0.3	
T	Temperature	150 °C	

Table I

	k_a^0 ($m^3\,mol^{-1}\,min^{-1}$)	k_d^0 ($m^3\,mol^{-1}\,min^{-1}$)	Ea_a ($J\,mol^{-1}$)	Ea_d ($J\,mol^{-1}$)	Ref.
Set 1 (Corn Stover)	1.4×10^{14}	3.3×10^{10}	111.6×10^3	95.7×10^3	(Qiang et al., 2011)
Set 2 (Bagasse)	1.3×10^9	1.6×10^{14}	82.8×10^3	118.9×10^3	(Lavarack et al., 2002)
Set 3 (Sweet Sorghum Bagasse)	3.53×10^6	0.62	60.7×10^3	14.5×10^3	(Liu et al., 2012)

Table II

List of Figures

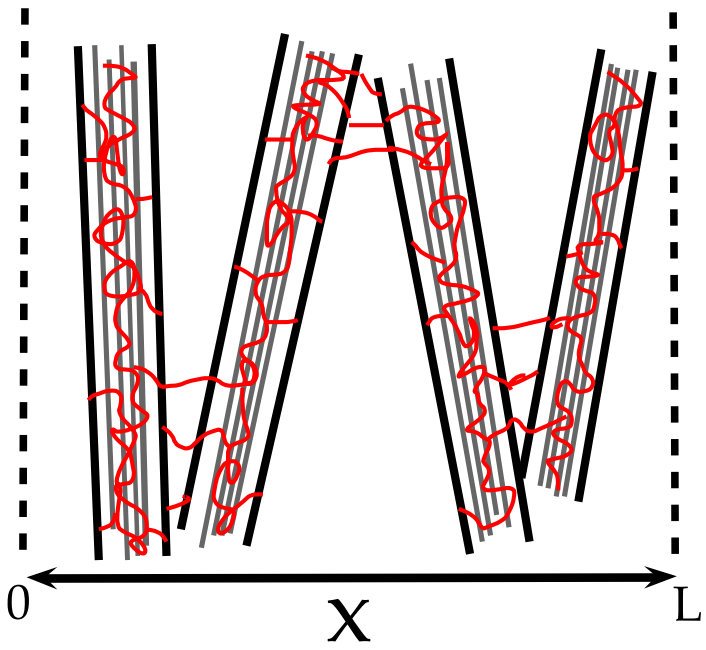

Figure 1

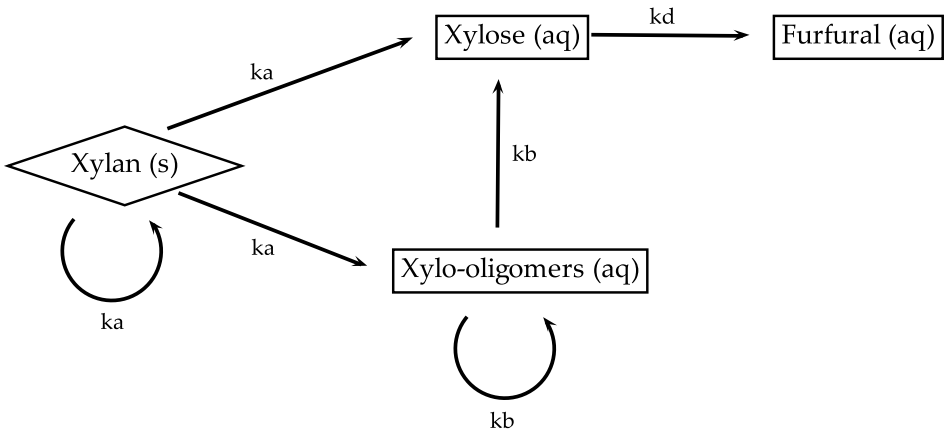
Xylose (aq)
kd
Furfural (aq)
ka
Xylan (s)
kb
ka
Xylo-oligomers (aq)
ka
kb

Figure 2

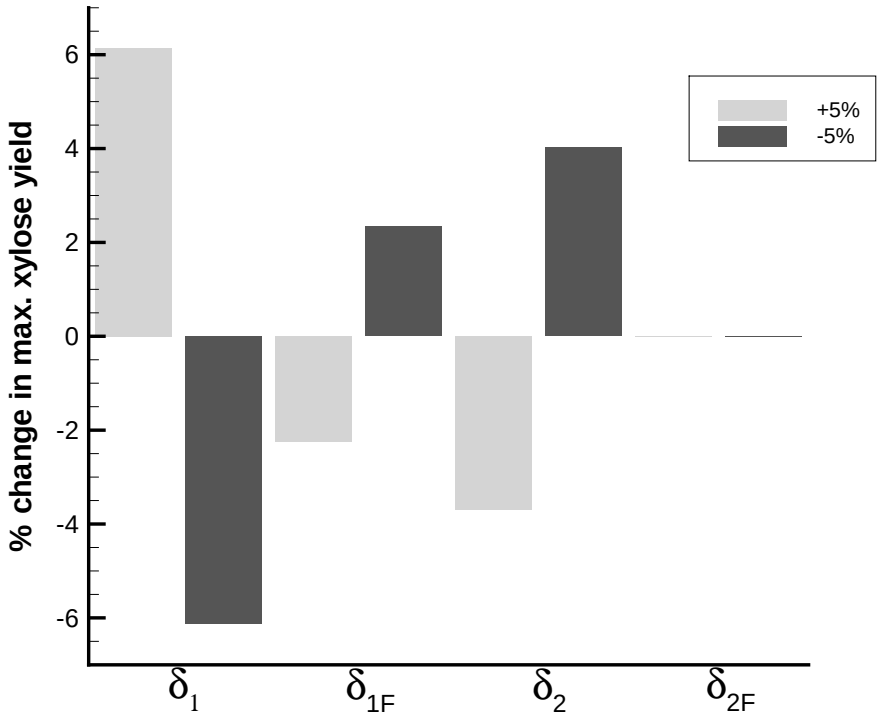

Figure 3

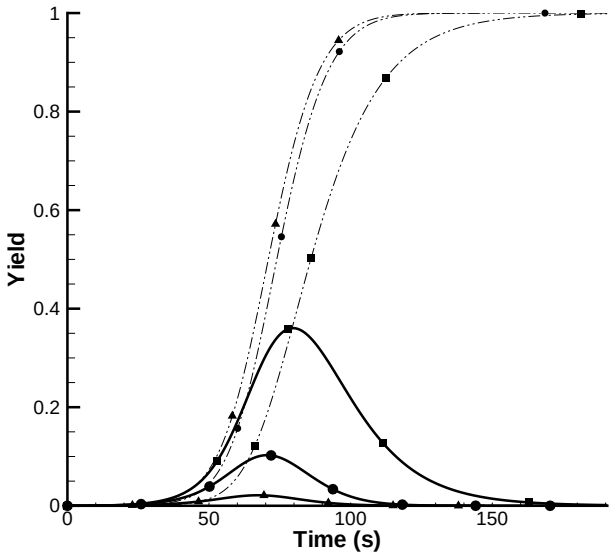

Figure 4

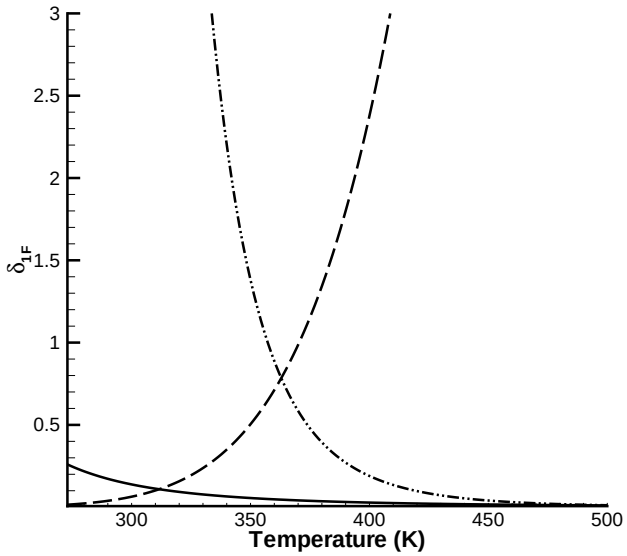

Figure 5

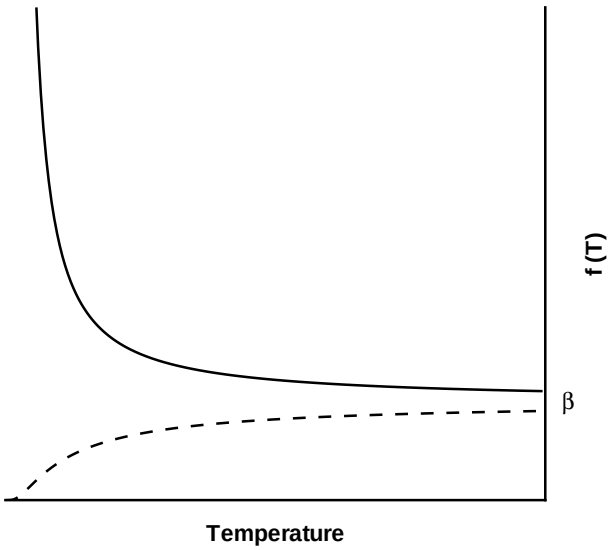

Figure 6

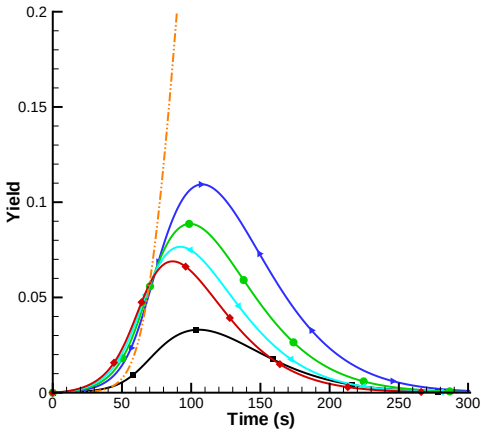

(a) $\delta_1 = 0.2$

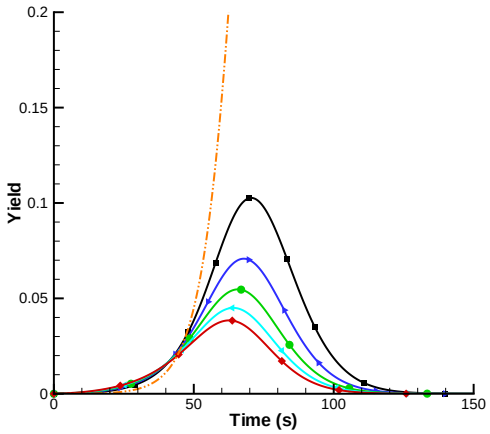

(b) $\delta_1 = 1$

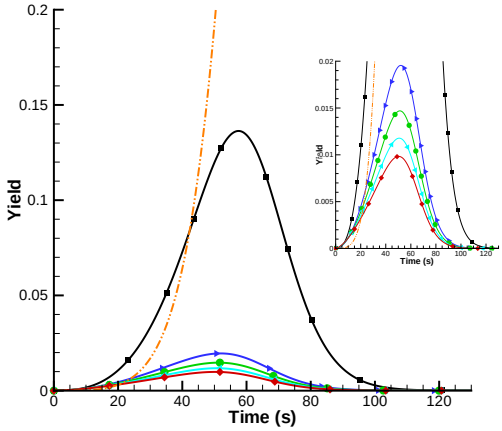

(c) $\delta_1 = 5$

Figure 7

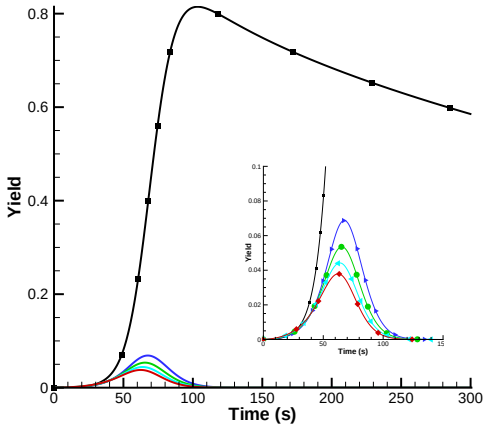

(a) $\delta_2 = 0.001$

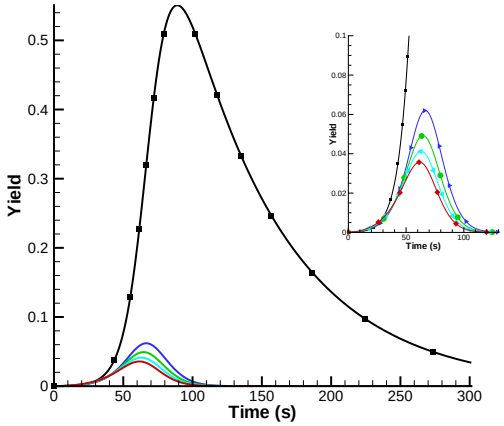

(b) $\delta_2 = 0.01$

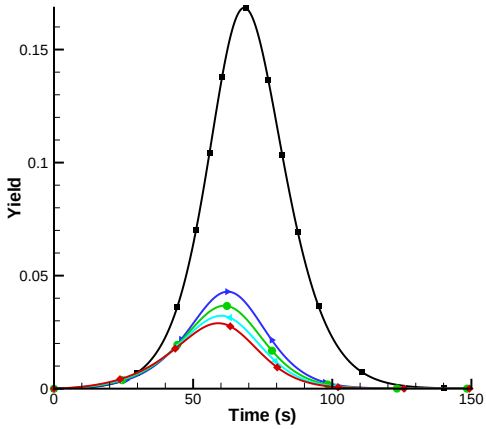

(c) $\delta_2 = 0.1$

Figure 8